ACS APPLIED MATERIALS & INTERFACES

www.acsami.org

Research Article

# Adsorptive Separation of Aromatic Compounds from Alkanes by $\pi-\pi$ Interactions in a Carbazole-Based Conjugated Microporous Polymer

Tongfan Chen, Wenxiang Zhang, Bin Li,* Wenbo Huang, Chunhui Lin, Yue Wu, Shuhui Chen, and Heping Ma*

Cite This: *ACS Appl. Mater. Interfaces* 2020, 12, 56385−56392

Read Online

ACCESS | Metrics & More | Article Recommendations | Supporting Information

**ABSTRACT:** Separation of aromatic/alkane mixtures of similar size and properties is critical for the chemical industry as conventional thermal separation is a high-cost and an energy-intensive process. Adsorptive separation based on porous materials is a prospective and economical technology as well as a suitable alternative to the energy-inefficient heat-driven separation process. With this in mind, we design and synthesize a novel microporous polymer (termed CMP-S-1) with a conjugated aromatic skeleton as a porous adsorbent for aromatic/alkane separation. CMP-S-1 possesses high aromatic adsorption selectivity in two representative separation systems (benzene vs cyclohexane and 3-methylthiophene vs *n*-octane) based on a vapor adsorption experiment and an ideal adsorbed solution theory simulation. The instant adsorption rate, adsorption energy calculations, and liquid fixed-bed breakthrough experiments give convincing demonstrations on the preferential selective adsorption of aromatic compounds over alkanes in CMP-S-1. The strong $\pi-\pi$ interaction between aromatics and the naphthalene ring is considered as the main reason for the strong affinity of aromatic compounds in the CMP-S-1 skeleton. The remarkable aromatic/alkane separation performance of CMP-S-1 verifies the important influence of the $\pi$-conjugation interaction in the conjugated porous polymer for the low-energy consumption adsorption separation process.

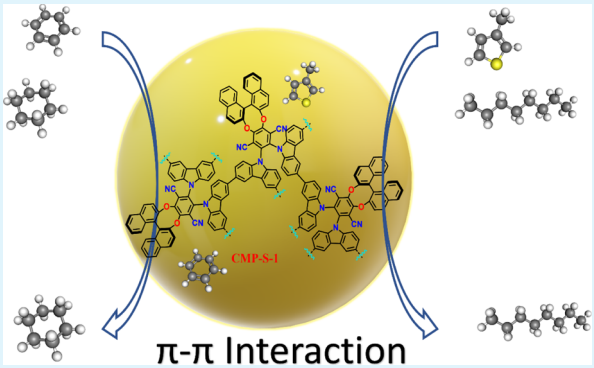


**KEYWORDS:** *porous framework, conjugated microporous polymers, adsorption separation, desulfurization, $\pi-\pi$ interaction*



## 1. INTRODUCTION

Separation of aromatics from saturated alkanes is an essential technology in the chemical industry as hydrogenation processes are frequently used in petroleum refining and synthesis of important fine chemicals.[1] For instance, cyclohexane is usually produced by the catalytic hydrogenation of benzene, which accounts for 80−85% of the world's total cyclohexane production.[2] The separation of unreacted benzene from the productive benzene/cyclohexane stream is one of the most challenging tasks because of their close boiling points (benzene, 80.1 °C, vs cyclohexane, 80.7 °C) and the formation of an azeotropic mixture.[3] The conventional method for the separation of benzene/cyclohexane mixtures is extractive distillation or azeotropic distillation, which involves high-energy consumption accompanied by a high operating cost.[4] Another high-energy consuming separation operation in petroleum refining is the removal of aromatic sulfides from gasoline, which needs to meet stringent environmental regulations with an ultralow sulfur concentration in transportation fuels.[5] The widely used hydrodesulfurization (HDS) process is operated at elevated temperatures (300−340 °C) and pressures (20−100 atm. of $H_2$),[6] which also faced with the severely high cost and safety risk. Thus, developing a less energy-intensive technology to separate aromatics from hydrocarbons (benzene form cyclohexane and aromatic sulfides from gasoline) is highly needed for a sustainable chemical industry in the future.

Adsorptive separation using a porous adsorbent is a promising low-energy consumption alternative as it can be accomplished at ambient temperatures and pressures. The current application of adsorptive separation in the chemical industry mainly focused on gas separation, such as pressure swing adsorption for hydrogen purification.[7] Using the adsorption technology to achieve liquid mixture separation is stagnant because of the poor performance of porous

Received: October 10, 2020
Accepted: November 24, 2020
Published: December 3, 2020

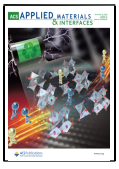




https://dx.doi.org/10.1021/acsami.0c18232
*ACS Appl. Mater. Interfaces* 2020, 12, 56385−56392

**Table 1. Physical−Chemical Parameters of Selected Adsorbates**

| compound | molecular weight (g·mol$^{-1}$) | boiling point (K) | molecular size/Å[12] | saturated vapor pressure (kPa) |
|---|---|---|---|---|
| benzene | 78.11 | 353.30 | 3.3 × 6.6 × 7.3 | 13.33 kPa at 26.0 °C |
| cyclohexane | 84.16 | 353.90 | 5.0 × 6.6 × 7.2 | 13.33 kPa at 25.5 °C |
| 3-methylthiophene[a] | 98.17 | 387.15 | 3.3 × 5.2 × 6.4 | 5.64 kPa at 37.7 °C |
| *n*-octane[a] | 114.23 | 398.75 | 3.2 × 3.9 × 10.9 | 4.00 kPa at 39.3 °C |

[a]3-Methylthiophene is the main aromatic sulfide in gasoline, and *n*-octane was selected to simulate gasoline.

adsorbents in the liquid phase, especially for the separation of benzene/cyclohexane and aromatic sulfide/gasoline with similar physical properties (Table 1). Recently, some metal−organic frameworks (MOFs) have been exploited for benzene−cyclohexane separation[8,9] and adsorption desulfurization in gasoline.[10,11] Their large surface areas and adjustable pore surface properties make MOFs good candidates for liquid phase adsorptive separation. However, the upscaling of MOFs is expensive as it depends on special ligand/metal components and strict synthetic conditions (usually in a solvothermal reaction). Moreover, the coordination bond nature of MOFs makes their stability and durability in harsh chemical environments still skeptical.

Porous organic frameworks (POFs) emerging as a new class of nanoporous polymers have attracted wide attention in materials science.[13] Following reticular chemistry construction principles that have been especially fruitful in MOFs, POFs can also realize customized functionalities by accommodating organic building blocks and linked covalent bonds. Based on this principle, many POFs have been developed such as covalent organic frameworks (COFs),[14,15] crystalline triazine-based frameworks (CTFs),[16,17] porous aromatic frameworks (PAFs),[18,19] hypercross-linked polymers (HCPs),[20,21] conjugated microporous polymers (CMPs),[22,23] and so on. The mature polymerization reaction and stable covalent bond nature make POFs very attractive in becoming a next-generation porous adsorbent. In these POFs, conjugated microporous polymers with extended conjugated aromatic skeletons are ideal candidates for separating aromatics from saturated alkanes because of their adjustable $\pi$-electron conjugate structure and tuneable nanosize pore diameter. Moreover, the persistent porosity and interconnected pore structure of CMPs can minimize the diffusion resistance of the adsorbate, which is highly conducive to industrial liquid-phase-separation applications.

Herein, we designed a conjugated microporous polymer (named CMP-S-1) with a conjugated polycarbazole and an aromatic naphthalene group in the framework. The organic vapor adsorption experiments demonstrated that CMP-S-1 can adsorb more aromatic compounds compared with alkanes (benzene vs cyclohexane and 3-methylthiophene vs *n*-octane) accompanied by a high aromatic adsorption rate. Moreover, the wide extension conjugated aromatic skeletons in CMP-S-1 can increase the aromatic adsorption selectivity through the spatial configurational $\pi-\pi$ interaction between the conjugated naphthalene group and the planar $\pi$-cloud of aromatics. The kinetic breakthrough experiments also demonstrated that CMP-S-1 can separate aromatics from the hydrocarbon mixture efficiently through a liquid fixed-bed adsorption process.

## 2. EXPERIMENTAL SECTION

**2.1. Materials and Methods.** All reagents and solvents were purchased from Energy Chemical, Sinopharm Chemical Reagent Co., Ltd. and used without further purification. $^1$H NMR spectra were recorded on an AVANCE III 400 MHz NMR spectrometer (Bruker, Germany). Fourier-transform infrared spectroscopy (FT-IR) was performed on a Nicolet 380 spectrometer. X-ray diffraction patterns were acquired from 3 to 40° using a Bruker-AXS D8 Discover diffractometer. $N_2$ adsorption/desorption data were acquired on an ASAP2460 physisorption analyzer (Micromeritics, USA). Thermogravimetric analysis (TGA) was conducted using a thermal analysis system (NETZSCH STA 449 F3, Germany). The morphology of the samples was characterized using a field-emission scanning electron microscope (Nova NanoS 450). The adsorption isotherms and kinetics were analyzed with a gravimetry vapor sorption analyzer 3H-2000PW, Beishide Instrument Technology (Beijing) Co., Ltd.

**2.2. Synthesis of CMP-S-1.** The synthesis method that was used to prepare the monomer (S-1) was the same as previously reported.[24] The synthesis of CMP-S-1 was performed using a modified procedure reported by Han et al.[25] Under nitrogen gas protection, S-1 (0.74 g, 1.0 mmol) was dissolved in anhydrous chloroform (60 mL). The monomer solution was added dropwise to a mixture of anhydrous $FeCl_3$ (1.62 g, 10 mmol) and anhydrous chloroform (40 mL). The resulting reaction mixture was stirred for 3 days at room temperature. Methanol (200 mL) was added and stirred for 3 h to quench the reaction. The obtained polymers were washed with HCl (12 M) for 4 h, filtered, and washed with water and THF. The crude polymer was further purified by Soxhlet extraction with THF for 48 h and then dried at 120 °C overnight. Yield: 0.72 g (97%).

## 3. RESULTS AND DISCUSSION

**3.1. Characterization of CMP-S-1.** The synthetic route to CMP-S-1 is shown in Scheme 1. The chemical structures of monomer S-1 and CMP-S-1 were first studied by FT-IR

**Scheme 1. Synthetic Route to CMP-S-1**

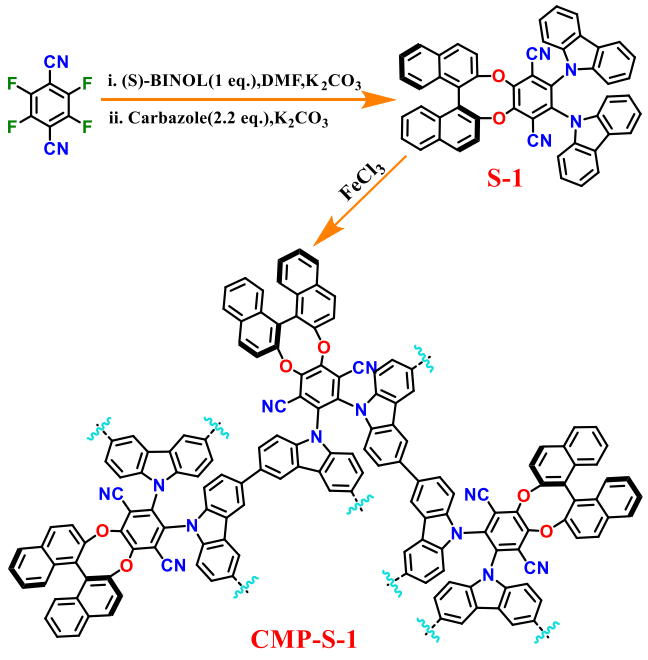



https://dx.doi.org/10.1021/acsami.0c18232
ACS Appl. Mater. Interfaces 2020, 12, 56385−56392

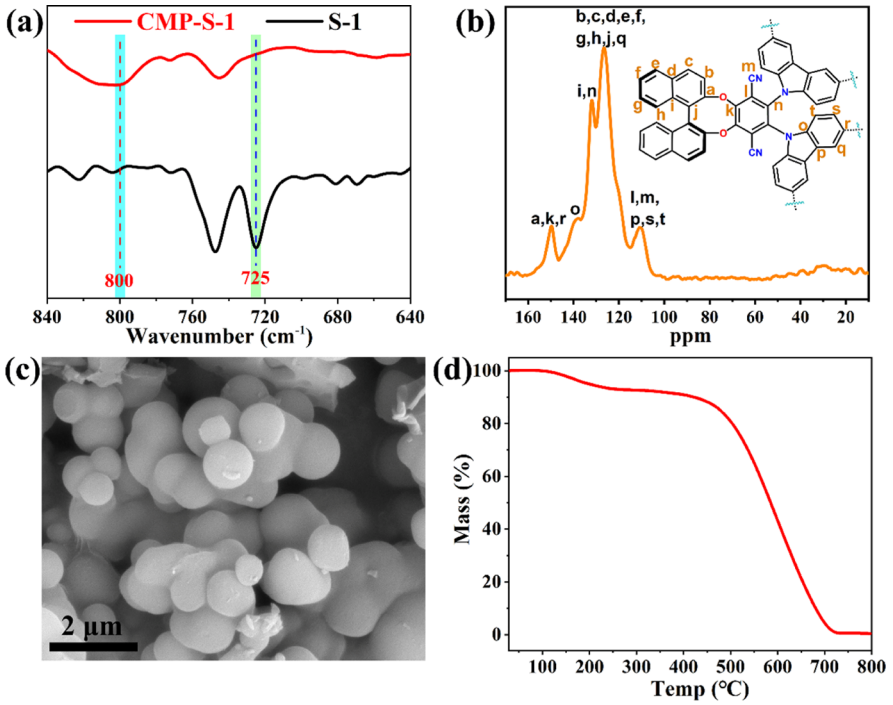


**Figure 1.** (a) FT-IR spectra of CMP-S-1; (b) solid-state $^{13}C$ CP/MAS NMR spectra of CMP-S-1; (c) SEM image of CMP-S-1; and (d) TGA curve of CMP-S-1.

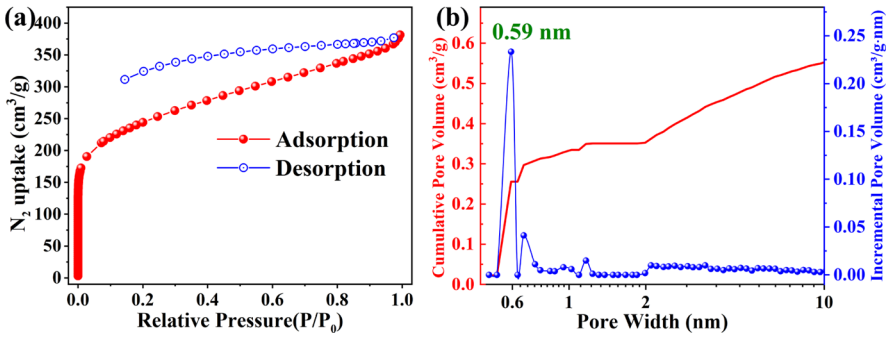


**Figure 2.** (a) Adsorption and desorption isotherms of nitrogen at 77 K for CMP-S-1; (b) pore size distribution curves and cumulative pore volume obtained by the NLDFT method for CMP-S-1.

(Figure S1). The vibration absorption peaks in S-1 at 3050 $cm^{-1}$ can be assigned to the aromatic C−H. The 2236 and 1263 $cm^{-1}$ vibration peaks are assigned to the −CN group and the C−O−C bonds of binaphthol, respectively. In the zoom-in IR spectra of S-1 and CMP-S-1 in Figure 1a the peak at 725 $cm^{-1}$ of S-1 disappeared and a new peak is observed at 800 $cm^{-1}$, which means that the carbazoles in CMP-S-1 are cross-linked.[26] The $^{13}C$ solid-state CP/MAS NMR spectra of CMP-S-1 are shown in Figure 1b. The chemical shifts at 150 ppm correspond to the carbons linked with O and N in CMP-S-1. The carbon chemical shift of cyanopyridine is at around 115 ppm. The peaks at 132, 126, and 110 ppm corresponded to other substituted phenyl carbons, including the naphthalene and carbazole. The morphology of CMP-S-1 was analyzed with a field-emission scanning electron microscope. As shown in Figure 1c, the obtained CMP-S-1 has an irregular spherical stacked morphology with hierarchical porosity. The thermal stability of CMP-S-1 was investigated by TGA. The TGA curve in Figure 1d exhibited a slight decrease in the temperature range from 120 to 250 °C, attributed to the removal of adsorbed water that existed in the pore. The resulting guest-free CMP-S-1 is thermally stable up to 450 °C as the weight remains unchanged between 250 and 450 °C.

The porosity and the pore structure of CMP-S-1 were measured by nitrogen adsorption and desorption isotherms at 77 K. As shown in Figure 2a, the nitrogen uptake of CMP-S-1 increased rapidly in the low-pressure region, which is in line with the type I adsorption isotherm characteristics. The calculated Brunauer−Emmett−Teller (BET) specific surface area of CMP-S-1 is 873 $m^2/g$. The pore size distribution of CMP-S-1 was calculated based on nonlocal density functional theory (NLDFT). As shown in Figure 2b, the pore size of CMP-S-1 is mainly distributed at around 0.59 nm. The experimental pore volume of CMP-S-1 is 0.53 $cm^3 \cdot g^{-1}$, as calculated from $N_2$ adsorption isotherms at $P/P_0$ = 0.995.

**3.2. Vapor Adsorption Performance of CMP-S-1.** The conjugated porous framework and narrow pore distribution in CMP-S-1 drive us to investigate its aromatic and alkane vapor adsorption. The single-component vapor sorption experiments of benzene, cyclohexane, 3-methylthiophene, and *n*-octane


https://dx.doi.org/10.1021/acsami.0c18232
ACS Appl. Mater. Interfaces 2020, 12, 56385−56392

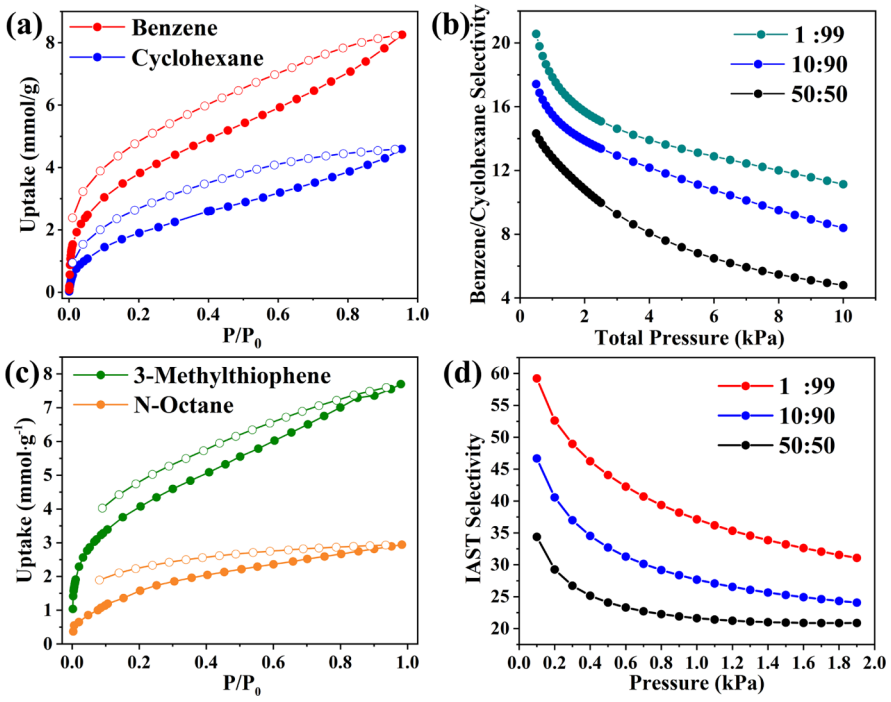


**Figure 3.** (a) Benzene/cyclohexane and (c) 3-methylthiophene/*n*-octane adsorption and desorption isotherms of CMP-S-1 at 298 K. Different ratios of (b) benzene/cyclohexane and (d) 3-methylthiophene/*n*-octane selectivity through IAST calculations.

were recorded with a gravimetry vapor sorption analyzer. As shown in Figure 3a,c, the vapor adsorption−desorption results of CMP-S-1 display larger aromatic adsorption capabilities (benzene and 3-methylthiophene) compared with the uptake of alkanes (cyclohexane and *n*-octane). The adsorption amount of benzene and 3-methylthiophene in CMP-S-1 is 8.3 and 7.7 mmol/g, respectively. For the cyclohexane and *n*-octane adsorption, CMP-S-1 shows low adsorption capacities with 4.5 mmol/g for cyclohexane and 2.9 mmol/g for *n*-octane. The obvious difference in the adsorption amount between aromatics and alkanes in CMP-S-1 indicates that CMP-S-1 has high affinity for aromatic compounds.

The adsorption selectivity of aromatics over alkanes in CMP-S-1 was evaluated using ideal adsorbed solution theory (IAST). We chose the dual site Langmuir−Freundlich model to fit the adsorption isotherm, and the selectivity was calculated at different mixed vapor ratios. As the relative content of aromatics fluctuated in a real productive stream, we change the proportion of aromatics in mixed vapors over a wide range of compositions from 1 to 50%. The corresponding IAST selectivity of benzene over cyclohexane and of 3-methylthiophene over *n*-octane is illustrated in Figure 3b,d, respectively. As shown in Figure 3b, for the 1:99 benzene/cyclohexane mixture, the benzene versus cyclohexane IAST selectivity is larger than 20 at low pressures and decreases slowly to 12 at higher pressures. As the proportion of benzene in the mixture increases, the selectivity of benzene over cyclohexane decreased. CMP-S-1 also exhibits high 3-methylthiophene adsorption selectivity over *n*-octane (Figure 3d). In a mixture containing 1 and 10% 3-methylthiophene, CMP-S-1 can selectively adsorb 3-methylthiophene with IAST selectivities of 59 and 47, respectively.

To further characterize the different affinity interactions between aromatics and alkanes in CMP-S-1, we performed molecular adsorption theoretical simulations to calculate the molecular position and adsorption energy in CMP-S-1. As shown in Figure 4, the conjugated molecules with a $\pi$−electron cloud (benzene and 3-methylthiophene) are parallel to planar

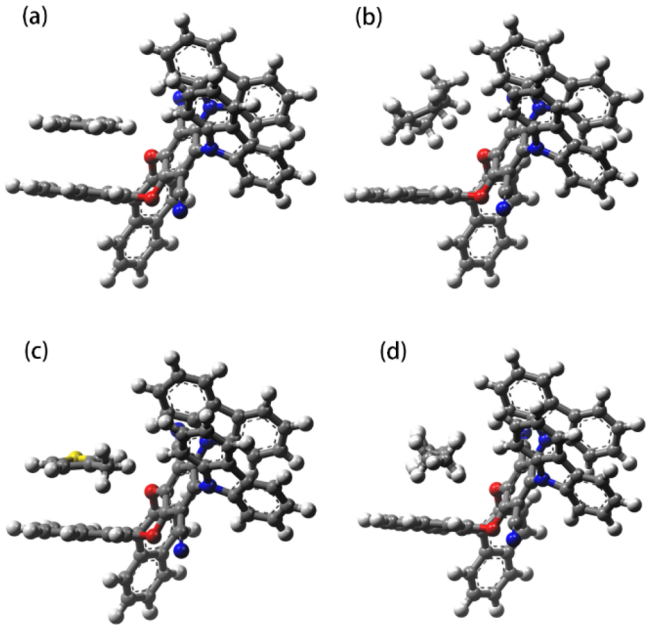


**Figure 4.** optimized adsorption sites of benzene (a), cyclohexane (b), 3-methylthiophene (c), and *n*-octane (d) on CMP-S-1 using Materials Studio.

naphthalene rings in CMP-S-1, but the alkanes without the $\pi$-conjugated structure (cyclohexane and *n*-octane) are in a random position. The adsorption energy ($\Delta E_{ads}$) during the adsorption process was calculated by adsorption locator modules using Materials Studio, and $\Delta E_{ads}$ values are listed in Table 2. According to the $\Delta E_{ads}$ results, $\Delta E_{ads}$ of benzene@CMP-S-1 (−0.87 eV) and 3-methylthiophene@CMP-S-1


https://dx.doi.org/10.1021/acsami.0c18232
ACS Appl. Mater. Interfaces 2020, 12, 56385−56392

**Table 2. Adsorption Energies of Different Vapors Adsorbed at CMP-S-1**

| | Bz@CMP-S-1 | Cy@CMP-S-1 | 3-mThio@CMP-S-1 | *n*-octane@CMP-S-1 |
|---|---|---|---|---|
| $\Delta E_{ads}$ | −0.87 eV | −0.53 eV | −0.82 eV | −0.69 eV |
| distance | 3.41 Å | 4.28 Å | 3.56 Å | 3.76 Å |

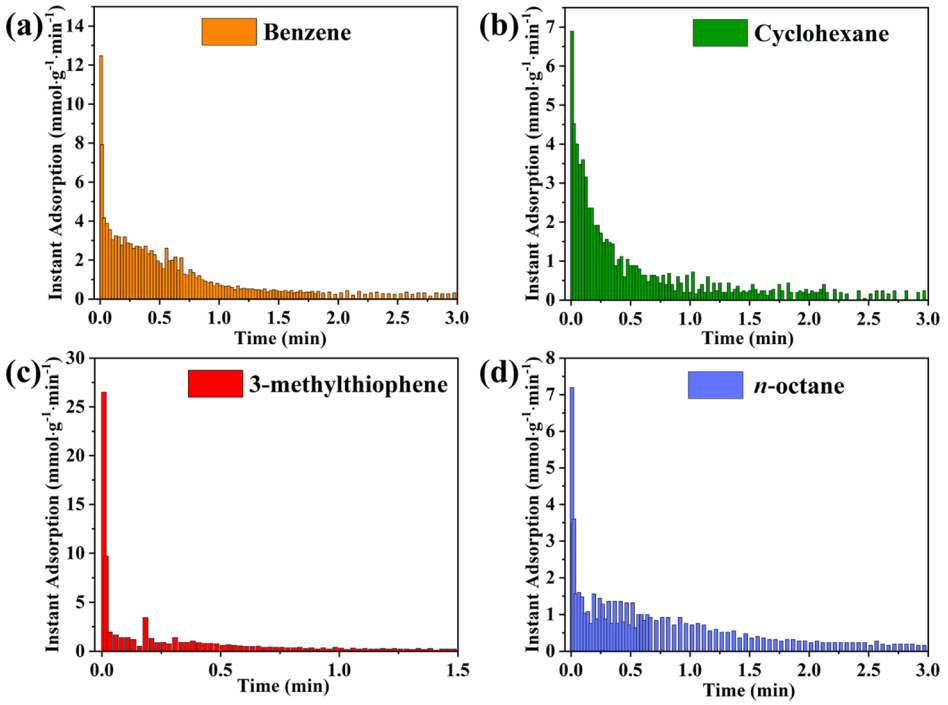


**Figure 5.** Instant adsorption rates of (a) benzene; (b) cyclohexane; (c) 3-methylthiophene; and (d) *n*-octane at 298 K.

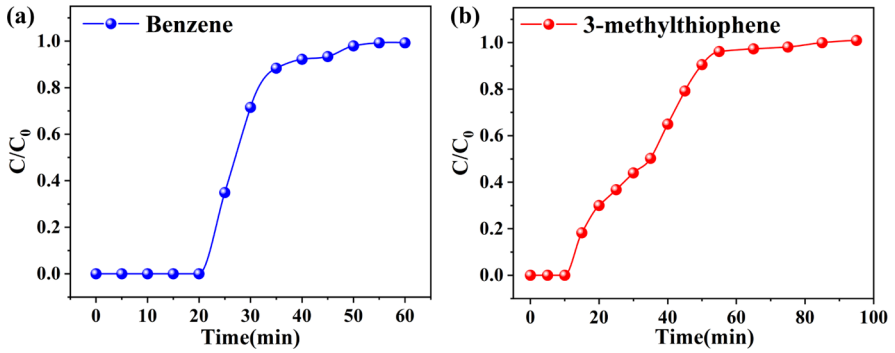


**Figure 6.** Fixed-bed breakthrough curves of (a) benzene and (b) 3-methylthiophene.

(−0.82 eV) are much lower than those of cyclohexane@CMP-S-1 (−0.53 eV) and *n*-octane@CMP-S-1 (−0.69 eV). The distance between the adsorbate molecules and naphthalene rings of CMP-S-1 is also listed in Table 2. Benzene and 3-methylthiophene with a conjugated $\pi$-cloud can form $\pi-\pi$ stacking interactions with the naphthalene rings in the CMP-S-1 framework with distances less than 3.6 Å. In comparison, for nonplanar cyclohexane and *n*-octane without delocalized $\pi$-bonds, there are no $\pi-\pi$ interactions in CMP-S-1. Therefore, the distances between alkane molecules and CMP-S-1 are larger than 3.7 Å.

**3.3. Instantaneous Adsorption Rates of Benzene/Cyclohexane and 3-Methylthiophene/*n*-Octane in CMP-S-1.** The time-dependent aromatic and alkane adsorptions on CMP-S-1 were measured at 25 °C. The results of instantaneous adsorption rates for benzene/cyclohexane and 3-methylthiophene/*n*-octane are shown in Figure 5. CMP-S-1 exhibited the maximum adsorption rate in the beginning for all vapors, then the adsorption rate decreased gradually along with the increase of adsorption time. The kinetic adsorption of benzene and cyclohexane is shown in Figure 5a,b. It is clear that CMP-S-1 exhibits much higher adsorption rate [12.5 mmol/(g·min)] for benzene than that of cyclohexane [6.9 mmol/(g·min)]. The maximum adsorption rate of 3-methylthiophene on CMP-S-1 was as high as 26 mmol/(g·min), which outperforms that of *n*-octane with 7.2 mmol/(g·min). It is worth mentioning that the adsorption rates of aromatics were much faster than those of alkanes during the whole test time, which means that aromatics can preferentially adsorb on CMP-S-1 and occupy the pores, resulting in high adsorption selectivity over alkanes.


https://dx.doi.org/10.1021/acsami.0c18232
ACS Appl. Mater. Interfaces 2020, 12, 56385−56392

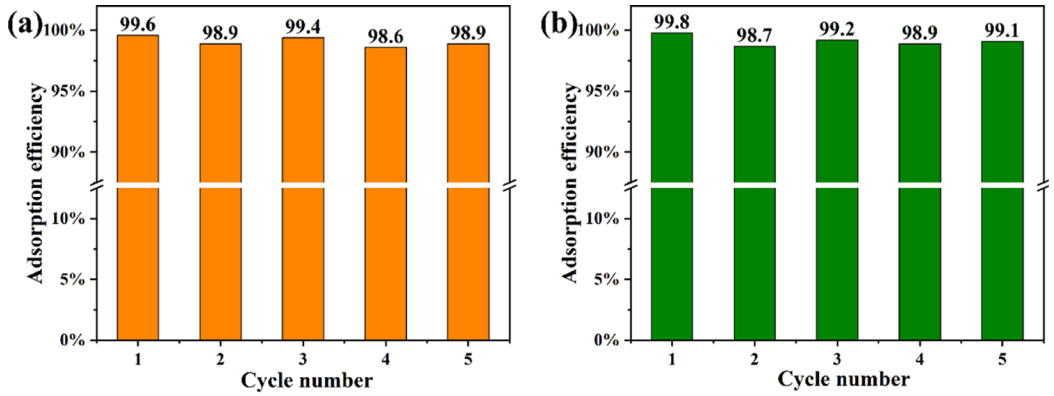


**Figure 7.** Benzene (a) and 3-methylthiophene (b) adsorption efficiencies of five cycle experiments of CMP-S-1.

**3.4. Fixed-Bed Liquid Mixture Breakthrough Experiments.** To further explore the aromatic/alkane separation performance of CMP-S-1 in practical separation processes, we designed a fixed-bed liquid mixture breakthrough experiment under dynamic conditions. We prepared two mixture solutions: 500 ppm 3-methlythiophene in *n*-octane to simulate the sulfur content in gasoline and 1% benzene in cyclohexane to simulate the benzene content in the cyclohexane production process. The breakthrough tests were performed using a fixed-bed column packed with CMP-S-1. The column pressure was controlled at 0.2 MPa. Mixed benzene/cyclohexane or 3-methylthiophene/*n*-octane solution gradually permeated and passed through the fixed bed, and the effluent was analyzed with a gas chromatograph at 5 min intervals. The breakthrough curves are presented in Figure 6.

For benzene/cyclohexane separation, the cyclohexane penetrated through the fixed bed first. Within 20 min, the CMP-S-1 column adsorbed benzene and yielded an outflow of pure cyclohexane. From 20 to 55 min, the benzene concentration in the outflow increased fast, and after about 55 min, the benzene was adsorbed to saturation in the bed. For the 3-methylthiophene/*n*-octane breakthrough experiment, *n*-octane was eluted through the CMP-S-1 bed in the first 15 min. After 50 min, 3-methylthiophene recovered to the initial concentration $C_0$.

**3.5. Evaluation of the Regeneration Performance of CMP-S-1.** In order to evaluate the regeneration ability of CMP-S-1 in the adsorption−desorption cycles, the following two methods were used: (1) rinsing CMP-S-1 with MeOH and then heating at 80 °C under vacuum for 30 min and (2) heating the used CMP-1 at 120 °C under vacuum and then cooling down to 25 °C before the next adsorption measurement. Then, regenerated CMP-S-1 was used to conduct a series of adsorption−desorption circulation experiments. The results showed that the adsorption efficiency of CMP-S-1 retains 98.5% of the original capacity after five cycles under the two regeneration methods (Figure 7).

These results indicate that CMP-S-1 can efficiently trap aromatics from alkanes under dynamic conditions. It can be therefore concluded that the strong $\pi-\pi$ interactions between aromatics and the conjugated skeleton of CMP-S-1 play a dominant role in the aromatic compounds' separation processes.

## 4. CONCLUSIONS

In summary, a new conjugated polycarbazole porous framework termed CMP-S-1 was synthesized and its adsorptive separation property of aromatic compounds from alkanes was studied in detail. The high number of carbazole and naphthalene units in CMP-S-1 can produce a conjugated $\pi$-electron cloud on the pore surface, which result in a high affinity toward aromatic molecules. CMP-S-1 exhibited exceptional high benzene/cyclohexane and 3-methylthiophene/*n*-octane adsorption selectivity based on IAST simulations. Adsorption kinetic experiments and DFT calculations were also performed to understand the competitive adsorption between aromatics and alkanes in CMP-S-1. The instant adsorption rate and adsorption energy analyses gave convincing demonstrations on the preferential selective adsorption of aromatic compounds on CMP-S-1. The remarkable aromatic/alkane separation performance of CMP-S-1 verifies the important influence of $\pi$-conjugation interaction on the separation process. Our research not only provides a promising candidate for the aromatic/alkane separation applied in the industrial hydrogenation of benzene to cyclohexane and low-energy consumption adsorption desulfurization but also presents a strategy for the targeted synthesis of new porous materials with a specific conjugation group for adsorption separation.

## ■ ASSOCIATED CONTENT

### Supporting Information

The Supporting Information is available free of charge at https://pubs.acs.org/doi/10.1021/acsami.0c18232.

FT-IR spectra of the monomer, carbazole, S-BINOL, and TFTPN and selectivity comparison of various materials toward benzene/cyclohexane (PDF)

## ■ AUTHOR INFORMATION

### Corresponding Authors

**Bin Li** − *State Key Laboratory of Luminescence and Applications, Changchun Institute of Optics, Fine Mechanics and Physics, Chinese Academy of Sciences, Changchun 130033, P. R. China; University of Chinese Academy of Sciences, Beijing 100049, P. R. China*; Email: libinteacher@163.com

**Heping Ma** − *School of Chemical Engineering and Technology, Xi'an Jiaotong University, Xi'an 710049, P. R. China*; orcid.org/0000-0002-7551-2639; Email: maheping@mail.xjtu.edu.cn



https://dx.doi.org/10.1021/acsami.0c18232
ACS Appl. Mater. Interfaces 2020, 12, 56385−56392

### Authors

**Tongfan Chen** − *State Key Laboratory of Luminescence and Applications, Changchun Institute of Optics, Fine Mechanics and Physics, Chinese Academy of Sciences, Changchun 130033, P. R. China; University of Chinese Academy of Sciences, Beijing 100049, P. R. China*

**Wenxiang Zhang** − *School of Chemical Engineering and Technology, Xi'an Jiaotong University, Xi'an 710049, P. R. China*

**Wenbo Huang** − *State Key Laboratory of Luminescence and Applications, Changchun Institute of Optics, Fine Mechanics and Physics, Chinese Academy of Sciences, Changchun 130033, P. R. China; University of Chinese Academy of Sciences, Beijing 100049, P. R. China*

**Chunhui Lin** − *State Key Laboratory of Luminescence and Applications, Changchun Institute of Optics, Fine Mechanics and Physics, Chinese Academy of Sciences, Changchun 130033, P. R. China; University of Chinese Academy of Sciences, Beijing 100049, P. R. China*

**Yue Wu** − *School of Chemical Engineering and Technology, Xi'an Jiaotong University, Xi'an 710049, P. R. China*

**Shuhui Chen** − *School of Chemical Engineering and Technology, Xi'an Jiaotong University, Xi'an 710049, P. R. China*

Complete contact information is available at: https://pubs.acs.org/10.1021/acsami.0c18232


### Notes

The authors declare no competing financial interest.

## ■ ACKNOWLEDGMENTS

We acknowledge the support by the National Natural Science Foundation of China (grant no. 21773223, 21673218, and 51872281) and the Science and Technology Developing Project of Jilin Province (grant no. 20180101177JC and 20180101176JC), the Natural Science Basic Research Plan in Shaanxi Province of China (no. 2020JM-005 and 2020JQ-017), and the Fundamental Research Funds for the Central Universities (xzy012019027). Prof. Ma acknowledges financial support from the "Young Talent Support Plan" of Xi'an Jiaotong University (HG6J001) and "1000-Plan program" of Shaanxi Province. We also thank the Instrument Analysis Center of Xi'an Jiao Tong University for the assistance test. The authors also gratefully acknowledge Prof. Huanyu Zhao at Jilin University for help in getting access to the software of Materials Studio.

## ■ REFERENCES


(1) Zhou, J.; Yu, G.; Li, Q.; Wang, M.; Huang, F. Separation of Benzene and Cyclohexane by Nonporous Adaptive Crystals of a Hybrid[3]arene. *J. Am. Chem. Soc.* **2020**, *142*, 2228−2232.

(2) Yao, H.; Wang, Y. M.; Quan, M.; Farooq, M. U.; Yang, L. P.; Jiang, W. Adsorptive Separation of Benzene, Cyclohexene, and Cyclohexane by Amorphous Nonporous Amide Naphthotube Solids. *Angew. Chem., Int. Ed. Engl.* **2020**, *59*, 19945−19950.

(3) Dong, H.; Yang, X.; Yue, G.; Cao, W.; Zhang, J. Liquid−Liquid Equilibria for Benzene + Cyclohexane +N,N-Dimethylformamide + Ammonium Thiocyanate. *J. Chem. Eng. Data* **2011**, *56*, 2664−2668.

(4) Li, W.; Xu, B.; Lei, Z.; Dai, C. Separation of benzene and cyclohexane by extractive distillation intensified with ionic liquid. *Chem. Eng. Process* **2018**, *126*, 81−89.

(5) Shirazinia, S. R.; Semnani, A.; Nekoeinia, M.; Shirani, M.; Akbari, A. Novel sustainable metal complex based deep eutectic solvents for extractive desulphurisation of fuel. *J. Mol. Liq.* **2020**, *301*, 112364.

(6) Yang, R. T.; Hernández-Maldonado, A. J.; Yang, F. H. Desulfurization of Transportation Fuels with Zeolites Under Ambient Conditions. *Science* **2003**, *301*, 79.

(7) Jiang, J.-X.; Su, F.; Trewin, A.; Wood, C. D.; Campbell, N. L.; Niu, H.; Dickinson, C.; Ganin, A. Y.; Rosseinsky, M. J.; Khimyak, Y. Z.; Cooper, A. I. Conjugated Microporous Poly(aryleneethynylene) Networks. *Angew. Chem., Int. Ed. Engl.* **2007**, *46*, 8574−8578.

(8) Mukherjee, S.; Manna, B.; Desai, A. V.; Yin, Y.; Krishna, R.; Babarao, R.; Ghosh, S. K. Harnessing Lewis acidic open metal sites of metal-organic frameworks: the foremost route to achieve highly selective benzene sorption over cyclohexane. *Chem. Commun.* **2016**, *52*, 8215−8218.

(9) Manna, B.; Mukherjee, S.; Desai, A. V.; Sharma, S.; Krishna, R.; Ghosh, S. K. A $\pi$-electron deficient diaminotriazine functionalized MOF for selective sorption of benzene over cyclohexane. *Chem. Commun.* **2015**, *51*, 15386−15389.

(10) Peralta, D.; Chaplais, G.; Simon-Masseron, A.; Barthelet, K.; Pirngruber, G. D. Metal-organic framework materials for desulfurization by adsorption. *Energy Fuels* **2012**, *26*, 4953−4960.

(11) Hao, L.; Hurlock, M. J.; Ding, G.; Zhang, Q. Metal−Organic Frameworks Towards Desulfurization of Fuels. In *Metal-Organic Framework*; Springer, 2020; pp 175−202.

(12) Lin, C.; Cheng, Z.; Li, B.; Chen, T.; Zhang, W.; Chen, S.; Yang, Q.; Chang, L.; Che, G.; Ma, H. High-Efficiency Separation of Aromatic Sulfide from Liquid Hydrocarbon Fuel in Conjugated Porous Organic Framework with Polycarbazole Unit. *ACS Appl. Mater. Interfaces* **2019**, *11*, 40970−40979.

(13) Das, S.; Heasman, P.; Ben, T.; Qiu, S. Porous Organic Materials: Strategic Design and Structure-Function Correlation. *Chem. Rev.* **2017**, *117*, 1515−1563.

(14) Kandambeth, S.; Dey, K.; Banerjee, R. Covalent organic frameworks: chemistry beyond the structure. *J. Am. Chem. Soc.* **2018**, *141*, 1807−1822.

(15) Geng, K.; He, T.; Liu, R.; Dalapati, S.; Tan, K. T.; Li, Z.; Tao, S.; Gong, Y.; Jiang, Q.; Jiang, D. Covalent Organic Frameworks: Design, Synthesis, and Functions. *Chem. Rev.* **2020**, *120*, 8814−8933.

(16) Yang, Z.; Wang, S.; Zhang, Z.; Guo, W.; Jie, K.; Hashim, M. I.; Miljanić, O. Š.; Jiang, D.-e.; Popovs, I.; Dai, S. Influence of fluorination on $CO_2$ adsorption in materials derived from fluorinated covalent triazine framework precursors. *J. Mater. Chem. A* **2019**, *7*, 17277−17282.

(17) Kuhn, P.; Antonietti, M.; Thomas, A. Porous, Covalent Triazine-Based Frameworks Prepared by Ionothermal Synthesis. *Angew. Chem., Int. Ed. Engl.* **2008**, *47*, 3450−3453.

(18) Tian, Y.; Zhu, G. Porous Aromatic Frameworks (PAFs). *Chem. Rev.* **2020**, *120*, 8934−8986.

(19) Ben, T.; Pei, C.; Zhang, D.; Xu, J.; Deng, F.; Jing, X.; Qiu, S. Gas storage in porous aromatic frameworks (PAFs). *Energy Environ. Sci.* **2011**, *4*, 3991−3999.

(20) Ramezanipour Penchah, H.; Ghaemi, A.; Ganadzadeh Gilani, H. Benzene-Based Hyper-Cross-Linked Polymer with Enhanced Adsorption Capacity for $CO_2$ Capture. *Energy Fuels* **2019**, *33*, 12578−12586.

(21) Ramezanipour Penchah, H.; Ghanadzadeh Gilani, H.; Ghaemi, A. $CO_2$, $N_2$, and $H_2$ Adsorption by Hyper-Cross-Linked Polymers and Their Selectivity Evaluation by Gas-Solid Equilibrium. *J. Chem. Eng. Data* **2020**, *65*, 4905−4913.

(22) Ma, L.; Liu, Y.; Liu, Y.; Jiang, S.; Li, P.; Hao, Y.; Shao, P.; Yin, A.; Feng, X.; Wang, B. Ferrocene-Linkage-Facilitated Charge Separation in Conjugated Microporous Polymers. *Angew. Chem., Int. Ed. Engl.* **2019**, *58*, 4221−4226.

(23) Yang, S.-J.; Ding, X.; Han, B.-H. Conjugated Microporous Polymers with Extended $\pi$-Structures for Organic Vapor Adsorption. *Macromolecules* **2018**, *51*, 947−953.

(24) Feuillastre, S.; Pauton, M.; Gao, L.; Desmarchelier, A.; Riives, A. J.; Prim, D.; Tondelier, D.; Geffroy, B.; Muller, G.; Clavier, G.; Pieters, G. Design and Synthesis of New Circularly Polarized

Thermally Activated Delayed Fluorescence Emitters. *J. Am. Chem. Soc.* **2016**, *138*, 3990−3993.
(25) Chen, Q.; Luo, M.; Hammershøj, P.; Zhou, D.; Han, Y.; Laursen, B. W.; Yan, C.-G.; Han, B.-H. Microporous polycarbazole with high specific surface area for gas storage and separation. *J. Am. Chem. Soc.* **2012**, *134*, 6084−6087.
(26) Zhang, X.; Lu, J.; Zhang, J. Porosity Enhancement of Carbazolic Porous Organic Frameworks Using Dendritic Building Blocks for Gas Storage and Separation. *Chem. Mater.* **2014**, *26*, 4023−4029.



https://dx.doi.org/10.1021/acsami.0c18232
*ACS Appl. Mater. Interfaces* 2020, 12, 56385−56392